Quarterly Reviews of Biophysics

www.cambridge.org/qrb

Review

Cite this article: Gordon R, Peters M and Ying C (2024). Optical scattering methods for the label-free analysis of single biomolecules. *Quarterly Reviews of Biophysics*, **57**, e12, 1–13
https://doi.org/10.1017/S0033583524000088

Received: 12 March 2024
Revised: 05 June 2024
Accepted: 19 June 2024

Keywords:
biotechnology; molecular dynamics of nucleic acids and proteins; protein biophysics; single-molecule sensing; light scattering

Corresponding author:
Reuven Gordon;
Email: rgordon@uvic.ca

CAMBRIDGE
UNIVERSITY PRESS

Optical scattering methods for the label-free analysis of single biomolecules

Reuven Gordon[1], Matthew Peters[1] and Cuifeng Ying[2]

[1]Department of Electrical Engineering, University of Victoria, Victoria, BC, Canada and [2]Advanced Optics and Photonics Laboratory, Department of Engineering, School of Science & Technology, Nottingham Trent University, Nottingham, UK

Abstract

Single-molecule techniques to analyze proteins and other biomolecules involving labels and tethers have allowed for new understanding of the underlying biophysics; however, the impact of perturbation from the labels and tethers has recently been shown to be significant in several cases. New approaches are emerging to measure single proteins through light scattering without the need for labels and ideally without tethers. Here, the approaches of interference scattering, plasmonic scattering, microcavity sensing, nanoaperture optical tweezing, and variants are described and compared. The application of these approaches to sizing, oligomerization, interactions, conformational dynamics, diffusion, and vibrational mode analysis is described. With early commercial successes, these approaches are poised to have an impact in the field of single-molecule biophysics.

Table of contents

Introduction **1**
Light scattering 2
Nanoplasmonic scattering 4
Applications **5**
Sizing 5
Oligomers and assembly 7
Interactions 8
Conclusions and outlook **9**

Introduction

Heterogeneity is abound for biomolecules; even nominally identical proteins have folding variations, conformational changes, and post-transcription modifications and exist at various stages of the enzymatic cycle (Martin-Baniandres *et al.*, 2023). With single-molecule approaches, it is possible to resolve these differences as well as observe dynamics without the need for synchronization (Moerner, 2002; Eisenstein, 2012; Ha, 2014; Miller *et al.*, 2017). It is possible to observe variations particular to the location or interaction state of a biomolecule and observe new or rare events that are obscured by ensemble averaging. Single-molecule studies are also the pinnacle of sensitivity and allow for analysis in crowded physiological environments. Single-molecule methods can observe interaction kinetics at equilibrium by relying on discrete "on" and "off" events, whereas ensemble measurements monitor the approach towards an equilibrium point (Al Balushi and Gordon, 2014b; Fineberg *et al.*, 2020).

Among optical methods, fluorescence has played a dominant role in the analysis of single biomolecules. Fluorescence-based methods have allowed for analysis of super-resolution structural information, particle tracking, folding/unfolding dynamics, and interactions (Chung *et al.*, 2012; Diezmann *et al.*, 2017). Despite this overwhelming success, attaching fluorescent labels can significantly modify the biophysics. Surface plasmon resonance studies have shown a 3–4 times difference in the equilibrium dissociation constants with streptavidin-peptide binding upon labelling with Cy3 (YS Sun *et al.*, 2008). Competitive binding studies have also shown variations in dissociation constants (up to two orders of magnitude) for DNA and proteins Dietz *et al.*, 2019. The impact varies with different fluorescent labels used in surface plasmon resonance imaging studies for binding to cells (Yin *et al.*, 2015). At the single-molecule level, using a hybrid plasmonic platform, changes were observed for DNA-protein interactions impacting the diffusion coefficient, the on and off binding rates, the surface potential, and molecular weight (Liang *et al.*, 2017). Labelling can introduce variations in protein dynamics (Weisgerber and Knowles, 2021), interactions with lipid bilayers (Hughes *et al.*, 2014), artefacts in tracking due to non-specific binding (Zanetti-Domingues *et al.*, 2013), and destabilization/collapse of proteins (Riback *et al.*, 2019).

In addition to modifying the biophysical properties, labelling adds complexity and cost: the labels have to be attached, and optical filters are required. Labelling limits observation time due to photobleaching and other effects. It also limits time resolution due to photon counting and precludes studies of species where labelling sites may not be known (or similarly, multiple labelling sites may be present, and so the attachment location is not deterministic). This may be complemented using X-ray crystallography and diffraction (Ringe and Petsko, 1985; Ilari and Savino, 2008) or by dynamic NMR (Kay, 2011) to get accurate protein structures, but this is highly specialized and inaccessible. Photobleaching impacts the time bandwidth, limiting the dynamic range between fastest and slowest timescales to three orders of magnitude (Schmid and Dekker, 2021). There have been improvements in labelling due to fluorescence fusion proteins (Luo *et al.*, 2020; Reja *et al.*, 2021). By genetically encoding fluorescent protein genes, proteins of interest can be fused with fluorescent tags, enabling real-time tracking of their dynamics and studying protein–protein interactions in the cellular environment. However, this technique requires the labels to be genetically encoded before protein expression, adding cost and complexity. With some fluorescence-based studies, there have been conflicting reports of conformational changes since Förster resonance energy transfer (FRET) relies on the fluorophore distance, which can be the same in different conformations (Hanson *et al.*, 2007; Henzler-Wildman *et al.*, 2007; Li *et al.*, 2015). Therefore, it is of interest to develop techniques that can observe biomolecules, their dynamics, and their interactions without fluorescent labels.

Techniques that avoid tethering to surfaces are similarly desired because tethering has been shown to hinder binding depending upon where the attachment is, and it also constrains the molecule against diffusion, which may alter the interaction or impact the molecular stability (Shental-Bechor and Levy, 2008; Grawe and Knotts, 2017). Simulations predicted that tethering in the wrong position can dramatically alter the folding of proteins (Arviv and Levy, 2012; Carmichael and Shell, 2015). Molecular dynamics simulations predicted either stabilization or destabilization of protein structure due to tethering (Levy, 2017). Tethering may modify the energy landscape of the protein domains (Busto, 1998). It was demonstrated experimentally that enzyme properties changed when immobilized to solid surfaces, leading to a decrease in its activity (Hanefeld *et al.*, 2013; Rodrigues *et al.*, 2013). Therefore, as with labelling, tethering can obstruct the natural structure and dynamics of proteins, and techniques that operate free from tethers can be explored to alleviate these points.

Optical scattering approaches are emerging as ways to measure single biomolecules and probe their dynamics, interactions, and properties. Methods that make use of direct scattering, like nanoparticle tracking analysis, are presently not sensitive enough to probe particles below 10 nm in size. Other methods can make use of shifts in resonances of microcavity, plasmonic, or hybrid platforms to enhance the sensitivity. They can also be based on interference scattering, making use of interference between a surface and particle scattering (iScat), or surface plasmon (surface plasmon resonance imaging – SPRi, plasmon scattering microscopy – PSM, or plasmon-enhanced protein tracking through interference – PEPTI) or a nanochannel in nanofluidic scattering microscopy (NSM) (Špačková *et al.*, 2022). Nanoaperture optical tweezers (NOTs) have emerged as a way to analyze single proteins in solution and make use of the optical forces to prevent the protein from diffusing away. Here, we will provide an overview of each of these techniques as well as describe their application in the study of proteins. Figure 1 shows schematic and representative data for various approaches to light scattering measurement of single proteins and other biomolecules.

Light scattering

The scattering of light from a single protein can be characterized by the polarizability, which is the ratio of the dipole moment to the electric field. The polarizability of an ellipsoid particle is given by:

$$\alpha = \epsilon_0 \epsilon_1 V \frac{(\epsilon_2 - \epsilon_1)}{L(\epsilon_2 - \epsilon_1) + \epsilon_1} \tag{1}$$

where V is the particle volume, ε_1 is the background relative permittivity, ε_2 is the particle relative permittivity, ε_0 is the free-space permittivity, L is the depolarization ratio, which for a prolate spheroid is:

$$L = \frac{1-\xi^2}{2\xi^3}\left(\ln\frac{1+\xi}{1-\xi} - 2\xi\right) \simeq \frac{1}{3} - \frac{2\xi^2}{15} - \frac{2\xi^4}{35} + O\left(\xi^6\right) \tag{2}$$

where $\xi = \sqrt{1 - \frac{b^2}{a^2}}$ and a and b are the major and minor axes.

From this equation, we can see that the elongated object of higher refractive index than the background (protein) has a higher polarizability since L decreases as the particle becomes more prolate from Eq. 2, and this can be used to obtain information about the shape and dynamic changes of a protein. For the case of a sphere $L = 1/3$; therefore, for roughly spherical proteins it has been found that the polarizability scales with the mass of the protein (Becker *et al.*, 2023):

$$\alpha = \delta\alpha \cdot m \tag{3}$$

which is expected since the polarizability scales with the volume. Published values for this proportionality for proteins have varied as 239 $Å^3$/kDa (Thiele *et al.*, 2023), 460 $Å^3$/kDa (Špačková *et al.*, 2022), and 724 $Å^3$/kDa (Becker *et al.*, 2023). This variation can be accounted for somewhat by whether the background permittivity is included in the polarizability of Eq. 1, but also is impacted by being close to a high refractive index substrate (Bobbert and Vlieger, 1987). Single- and double-stranded DNA have produced values that are 93% and 80% of these values (Li *et al.*, 2020).

For 445 nm laser, the scattering cross section of an average sized protein is 0.5×10^{-11} μm^2. So around 1 in 100 billion of the photons incident are scattered from a 0.5 micron squared spot (approximately the diffraction limit), and for 1 mW, this is 20,000 photons/second, with a comparable and typically larger count coming from surrounding regions. As a result, the signal is small, and homodyne (interference) detection schemes can be used to enhance the signal, as typified by interference scattering.

Interference scattering

iScat makes use of the interference between the scattering from a protein (or other object) at a surface and the surface itself (reference signal). This technique has been commercialized and is gaining widescale adoption as a protein characterization tool. The basic theory of how this operates is described below.

iScat signal The total scattered electric field can be written as:

$$E_t = E_r + E_s \tag{4}$$

where the subscripts r and s are for reference (from the surface) and scattered photons (from the protein). The intensity detected is proportional to the magnitude squared of this field:

$$I_t = I_r + I_s + 2|E_r E_s| cos\phi \tag{5}$$

https://doi.org/10.1017/S0033583524000088 Published online by Cambridge University Press

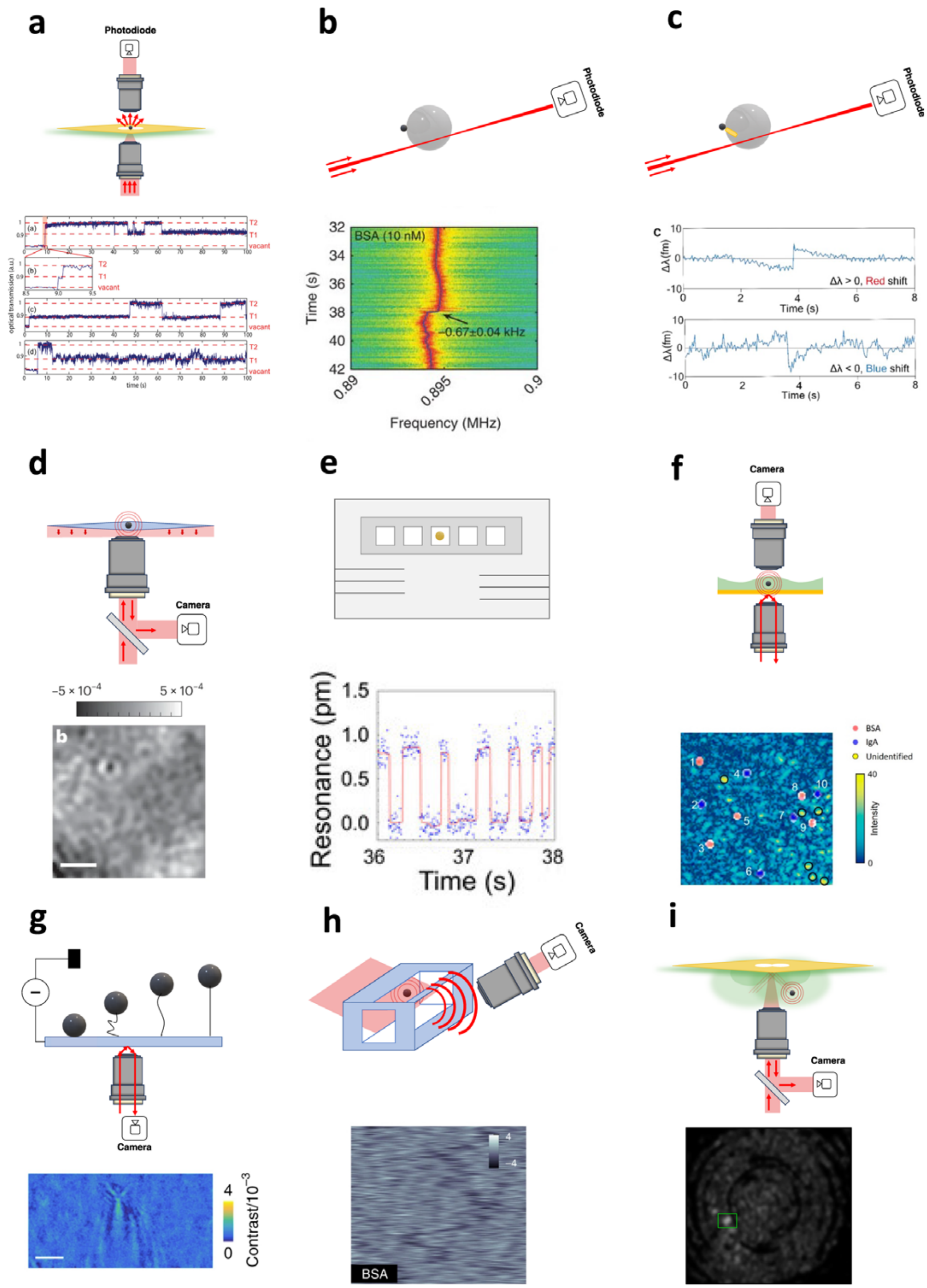

Figure 1. Simplified representations of label-free, single protein techniques and accompanied results with a ≈ 66 kDa protein. (**a**) Nanoaperture optical tweezers, schematic showing laser tweezer microscope with an aperture in a gold film where the transmission is monitored with representative trapping signal of Bovine Serum Albumin below (Pang and Gordon, 2012). (**b**) Whispering gallery mode, schematic showing evanescent coupling to spherical resonator through an optical fiber with a tunable laser and measurement of the intensity coupled via a photodiode upon attachment of a biomolecule, with representative frequency shift data shown below (Yu *et al.*, 2016). (**c**) Plasmonic-WGM, schematic showing introduction of gold nanorod to enhance sensitivity and representative wavelength shift data shown below (Note, 44 kDa protein shown) (Toropov *et al.*, 2023). (**d**) iScat (Dahmardeh *et al.*, 2023), schematic showing interference scattering from a biomolecule and surface observed by image subtraction on a camera, and a typical image subtraction shown below. (**e**) Photonic crystal-plasmonic hybrid (Liang *et al.*, 2017), schematic of a 1D photonic crystal cavity with a gold nanoparticle and protein-DNA interactions observed with single molecule sensitivity and representative frequency shift data shown below. (**f**) Plasmonic scattering microscopy, schematic showing total internal reflection excitation of surface plasmons and imaging from the top, with representative data shown below (Wan *et al.*, 2022). (**g**) Surface plasmon resonance imaging, showing illumination of a planar gold film exciting an evanescent wave that interferes with the scattering of a protein, imaged on the opposite side of illumination to remove the laser background, with a typical image of single proteins below (Ma *et al.*, 2020). (**h**) Nanofluidic scattering microscopy, schematic showing the diffusion of a protein through a nanochannel with interference between protein scattering and nanochannel scattering, accompanied by a representative time/position trace of bovine serum albumin below (Špačková *et al.*, 2022). (i) Plasmon enhanced protein tracking through interference, schematic showing the tracking of a single protein through interference of surface plasmon excited by scattering a laser off a nanoaperture with protein scattering, with representative image of a bovine serum albumin (Peters *et al.*, 2023).

where ϕ is the relative phase.

Since both the surface scattering and the protein scattering are proportional to the incident light, we can write this as $E_r = rE_i$ and $E_s = sE_i$. Usually the scattering is small so that the second term can be neglected in Eq. 5. In this limit, the shot noise is proportional to the square root of the reference signal, so that the signal to noise ratio is given by:

$$SNR = 2|s|E_i \tag{6}$$

which is twice the square root of the number of scattered photons and is proportional to α, or the protein mass. The reference signal can come from reflection off the surface that the protein lands on. A factor of $1/\sqrt{2}$ can be added to this relation to account for frame subtraction, which is used to detect changes when a protein lands on the surface (Becker *et al.*, 2023). As compared with dark-field approaches, where the reference field is removed and the signal is ideally coming from the scattered particle only, the SNR also scales as the scattered field, and so these should have similar limits of detection; however, practical implementations, such as nanoparticle tracking analysis (Filipe *et al.*, 2010), are limited to particles larger than 10 nm in size by undesired background scattering. Therefore, making use of the interference term has the primary practical benefit of increasing the signal relative to the unwanted background.

To detect the smallest objects, there are two considerations: maximize the signal to noise ratio by increasing the incident intensity so that as many scattered photons can be detected as possible, and do not saturate the detection or unduly increase background by reducing the reference intensity (Becker *et al.*, 2023). To reduce the reference signal, various apertures and attenuators have been used (Liebel *et al.*, 2017; Becker *et al.*, 2023). Integrating over time also increases the detected scattered photon number, at the expense of the time resolution Liebel *et al.*, 2017. In a well-engineered solution (Becker *et al.*, 2023), the typical time resolution of iScat is of the order of 0.1 second, and the typical smallest proteins that can be detected are 40 kDa (Becker *et al.*, 2023; Dahmardeh *et al.*, 2023), considering what is achievable experimentally. Proteins below 10 kDa are possible with machine learning, pushing the SNR close to 1 through anomaly detection (Becker *et al.*, 2023; Dahmardeh *et al.*, 2023). This surpasses the conventionally defined limit of detection given by SNR = 3 (Becker *et al.*, 2023). While the analysis has focused on the noise that is from the reference (mainly surface scattering), there is an additional time-varying noise from background speckle fluctuations and drift even in a pure water sample that limits the detection to around 5 kDa even with integration (Ortega Arroyo *et al.*, 2014; Liebel *et al.*, 2017; Dastjerdi *et al.*, 2021; Becker *et al.*, 2023). The signal is usually defined in terms of the contrast, which is $2|s|/|r|$. Variations in the local reflection from the surface change the signal, and this leads to reduced resolution that can be accounted for theoretically (Becker *et al.*, 2023). iScat has been commercialized by Refeyn, formed in 2018.

Plasmonic scattering microscopy, evanescent scattering microscopy and surface plasmon resonance imaging

In PSM, Kretschmann (total internal reflection) excitation of surface plasmon waves is used to excite scattering from nanoscale objects on a metal film. This approach combines the usual surface plasmon resonance geometry with microscopy, which makes use of interference scattering between the surface waves and the scattering, both from surface roughness and objects bound or immobilized at the surface (Zhang *et al.*, 2020). The surface plasmon waves are guided along the surface, and therefore not detected by the microscope above unless there is scattering out of the plane. Initial calibration of the approach showed a transition from sixth power size dependence expected from direct scattering to third power dependence expected from interference scattering as the particle size was reduced. The approach allows for discrete binding analysis of individual antibodies onto surfaces containing proteins, which makes use of established surface immobilization protocols for SPR (Zhang *et al.*, 2020). While SPR is not a tether-free technique, PSM and SPRi make use of tethering to image free-solution biomolecule binding. The sensing characteristics reported were SNR of 11 for IgA around 400 kDa with a 50 ms integration time, which is comparable to iScat. There was some indication that using a metal surface would make the approach sensitive to charge (Foley *et al.*, 2008; Shan *et al.*, 2010; Liu *et al.*, 2017); however, the impact of calcium ions with calmodulin was barely detectable at the single molecule level (Zhang *et al.*, 2020). Similar to plasmonic scattering, it is possible to use total internal reflection to scatter off of proteins at a surface without surface plasmons, and the interference with scattering off the rough surface can be used to detect the presence of individual proteins by image subtraction (Zhang *et al.*, 2022). The image is detected from above the surface, and the excitation field is incident from below.

SPRi uses the Kretschmann geometry, where both the exciting laser and imaged light are collected from below the sample. While SPRi predates PSM, the ability to resolve small particles with SPRi was not demonstrated until recently by integral scattering (Sun *et al.*, 2023). In that work, interference between the scattered field and the plasmon was used to extract the location and size of the scattering object, making use of a well-defined scattering pattern and wavevector filtering. The detection of BSA was achieved with SNR = 3, making this approach comparable to iScat. Earlier than this, oscillating a protein with a PEG linker to a surface allowed for "locking in" to the scattering signal at the oscillation frequency and thereby removing background noise. This allowed for detecting proteins as small as 14 kDa (Ma *et al.*, 2020).

Nanofluidic scattering microscopy

NSM again makes use of the interference between a protein to be tracked and a reference signal, except that the reference signal comes from scattering off of a nanochannel in glass that contains the protein (Špačková *et al.*, 2022). This makes use of dark-field excitation and allows for tracking diffusion of particles; that is, they do not have to land on the surface. Passivation of the surface with a supported lipid bilayer was used to allow for tracking positively charged nanoparticles; for negatively charged nanoparticles, interaction with the surface was rare.

Holography

While the common path configuration of iScat has inherent stability, it is possible to have the reference beam take a different pathway. This allows for holographic reconstruction that gives a greater tracking volume than nanoparticle tracking analysis (albeit for larger particles than proteins so far, and also at lower concentrations than typical for nanoparticle tracking analysis) (Ortiz-Orruño *et al.*, 2022). Stable phase extraction has been used with a four-camera approach for holographic extraction of single proteins (Thiele *et al.*, 2023). This first demonstration was still limited to fairly large proteins (∼90 kDa).

Nanoplasmonic scattering

Thermal effects

The ability to detect single protein binding events was demonstrated by backscattering from a single gold nanorod (Zijlstra *et al.*, 2012). In that work, the backscatter of a 693 nm (off resonance) laser from the nanorod with binding in the presence of a 785 nm heating laser (100 ms integration) was observed, as well as taking a full spectrum (15 *s* integration time). Plasmonic heating changes the local refractive index (photothermal effect), and this gives a larger wavelength shift than binding alone, which enabled the sensitivity to detect single streptavidin (53 kDa) binding. This technique allows you to adjust the sensitivity by making modifications in the heating laser power.

Nanoaperture optical tweezers

Optical tweezers use the changes in momentum of photons (light) scattered off an object to manipulate that object. Since this depends on the polarizability, large laser powers are required to trap small objects like single proteins, and this makes the approach impractical. The diffraction limit also makes the trapping volume large. Therefore, nanoapertures in metal films have been used to enhance the trapping efficiency and provide a smaller trapping volume. The double-nanohole/bowtie/coaxial-shaped apertures in metal films have been used by several groups to trap and analyze single proteins (Pang and Gordon, 2012; Yoo *et al.*, 2018; Peri *et al.*, 2019; Verschueren *et al.*, 2019; Ying *et al.*, 2021; Yang *et al.*, 2021). The continuous metal film surrounding the aperture helps to remove heat, and so typical temperature increases around 1 K/mW have been observed (Jiang *et al.*, 2020; Verschueren *et al.*, 2018; Xu *et al.*, 2018); this introduces a thermal gradient, which has a tendency to repel proteins (at room temperature or above) due to the typical positive Soret coefficient (thermophobic behavior). Nevertheless, the optical trapping potential can be large enough to allow trapping when a protein diffuses into the vicinity of the aperture under focused laser illumination.

The protein trapping is typically accompanied by a step in the transmitted power through the aperture. The transmitted power fluctuates due to thermal motion and conformational changes. The amplitude of the thermal fluctuations scales as the size of the particle being trapped Wheaton and Gordon, 2015. As with conventional optical tweezers, the power spectral density of these fluctuations has a corner frequency that scales as the trap stiffness divided by the drag. Since the trap stiffness is proportional to the polarizability, this also typically scales as the volume, and the Stokes drag scales as the radius, this gives a 2/3 power scaling of the corner frequency with mass, or $-2/3$ if we consider a characteristic timescale Wheaton and Gordon, 2015. Plasmon-enhanced protein-tracking through interference (PEPTI) allows for tracking the protein prior to trapping by a nanoaperture due to scattering (Peters *et al.*, 2023).

Microcavities and hybrid plasmonics

High-quality optical cavities have been investigated for label-free single protein detection by noting resonant shifts; however, initial reports were later revised to have not achieved the required sensitivity (Armani *et al.*, 2007; Lu *et al.*, 2011). A perturbation formulation can be used to estimate the wavelength shift of the resonance as well as the linewidth broadening (from the imaginary part) when a polarizable nanoparticle is introduced at position $\boldsymbol{r_i}$ (Arnold *et al.*, 2003):

$$\frac{\delta\omega}{\omega} \simeq \frac{-\alpha|\boldsymbol{E}(\boldsymbol{r_i})|^2}{2\int \epsilon|\boldsymbol{E}(\boldsymbol{r})|^2 dV} \tag{7}$$

where $\boldsymbol{E}(\boldsymbol{r})$ is the field of the unperturbed cavity at position $\boldsymbol{r}$. Strictly speaking, this integral is only valid for closed lossless systems and diverges for open cavities; this issue can be resolved by using quasinormal mode theory with the appropriate unconjugated orthogonality relations (Kristensen and Hughes, 2014; Wu *et al.*, 2021; Franke *et al.*, 2023).

Detection via frequency locking, or optomechanic effects, has improved the sensitivity to the single protein level (Su *et al.*, 2016; Yu *et al.*, 2016). By adding plasmonic nanoparticles or nanorods, it is possible to improve the sensitivity of these microcavities to the single DNA ($\sim$2 kDa) (Baaske *et al.*, 2014; Liang *et al.*, 2017), protein (Dantham *et al.*, 2013), and even single ion levels (Kim *et al.*, 2017). This arises because of the local field enhancement at the detection point with extreme subwavelength (plasmonic) localization. It is also possible, as noted with PSM, that charge is playing a role to shift the resonance through electrostatic interactions with the metal. A photonic-crystal plasmonic-particle cavity was used to establish the changes to the biophysical properties due to labelling at the single molecule level (Liang *et al.*, 2017). At higher powers, heating can take over and can have the opposite shift for hybrid platforms (Toropov *et al.*, 2023). Using a high-finesse fibre-based Fabry-Pérot microcavities and Pound-Drever-Hall cavity locking, detection of biomolecules down to a 1.2 kDa protein, Myc-tag, was achieved (Needham *et al.*, 2024). A 2D signal of temporal and intensity data allows this technique to distinguish between mixed protein samples and mixtures of DNA isomers of identical mass but different sequences. The detection relies on a refractive index change as the biomolecule displaces the water molecules of lower index, leading to resonance shifts of 1–49 kHz, 20 times greater than WGM resonator estimates. The high resolution is attributed to high passive stability, active low-frequency stabilization, creation of a velocity discrimination window, and the use of dynamic photothermal distortion of the resonance line shape.

Applications

The applications of light scattering single-molecule techniques to the label-free analysis of single proteins and other biomolecules are described in this section. Various biophysical parameters can be obtained through these techniques. Briefly, kinetic data such as protein oligomerization is obtainable via NOT, iScat, PEPTI, and holography; small molecule and antibody interactions with NOT, PC-Hybrid, SPRi, PSM, iScat, and WGM methods; and thermodynamic constants from NOT and PNP. When choosing which method to use in solving a specific question, one must consider not only the information desired but also the concentration range, temporal resolution, throughput, and accessibility of the technique. A technical comparison of the various approaches is given in Table 1.

Sizing

The relation between iScat contrast and mass was established by evaluating several proteins and other biomolecules landing on a glass surface (Young *et al.*, 2018). The mass derived from the contrast was accurate to within 5 kDa, and the precision for individual landing events was tens of kDa (Young *et al.*, 2018), which was later improved by accounting for local variations in the reflection of the glass interface to less than 10 kDa Becker *et al.*, 2023. The smallest protein detected was 53 kDa in the initial work (Young *et al.*, 2018), and this has been improved to below 10 kDa with machine learning, albeit with an accuracy of 5 kDa and precision of 60% (Dahmardeh *et al.*, 2023). It was possible to detect a change in the mass of streptavidin with

Table 1. Comparison of various label-free single biomolecule sensing techniques

	Detection limit		Concentration		Temporal resolution			Complexity			
Technique	Achieved	Fundamental	Low	High	Minimal Interval	Long-term observation?	High-throughput?	Resources	Expertise	Applications	Limitation(s)
WGM[1]	66 kDa	3.9 kDa (1σ)	10 nM	100 nM	256 ms	N	N	+++	+++	Single protein detection	Specialized expertise and resources Low throughput
WGM hybrid	24 kDa [2] 1 kDa[3]	–	Tethered		20 ms	Y (tethered)	N	+++	+++	Small molecule/ion interactions [3] Biochemical reactions[4,5] Ligand binding[6]	
NOT	4 kDa[7]	–	200 nM[a]	150 μM[8]	40 μs[9]	Y (1 h) [9]	N	+	+++	Protein sizing[8,10] Protein disassembly[11] Protein–protein(DNA) interactions [12,13] Small molecule/ion interactions[14–16] Antibody detection [12] Conformational dynamics[9,17] Vibrational modes[18]	Low throughput Long waiting time
iScat (Refeyn*)	30 kDa	–	100 pM*	100 nM*		N	Y	+	+	Protein sizing[19–21]*	Below physiological concentration[+]
iScat–ML[19]	9 kDa	5 kDa (1σ)	10 nM	10 nM	300 ms	N	Y	+	+++	Oligomerization/ assembly[21–23]*	
iScat–GNP [24]	170 kDa	–	Tethered		10 μs	Y (tethered)	N	++	++	Protein–protein(DNA) interactions[23,25–28]* Antibody detection[26]* Protein diffusion[29] Protein in live cell[30]	
PSM [31,32]	66 kDa[31]	25 kDa(3σ) [31]	0.1 nM [31,32]	20 nM [32]	50 ms[32]	Y (1 min [32] or tethered[33])	Y	++	++	Protein sizing[32–34] Antibody detection [31,32]	(PSM)Below physiological concentration (Opto–PSM) Low throughput Short observing duration
Opto–PSM [35]	64 kDa	15 kDa(1σ)	500 nM	8.7 μM	100 ns	N	N	+++	+++	Protein diffusion [35] Protein in live cell [36]	
SPRi[37]	17 kDa		Tethered		1 s	Y(tethered)	Y	+++	+++	Protein sizing Conformational changes Antibody detection	Tethering
NSM[38]	66 kDa	–	–	28 nM	5 ms	Y(seconds)[b]	Y	++	+++	Protein sizing Protein diffusion	Below physiological concentration
PEPTI[39]	14.3 kDa	–	–	69 μM	~ 30 ms	N	Y	+	+++	Protein sizing Protein diffusion	Low temporal resolution
PC–Hybrid[40]	31 kDa		Tethered		~ ms	Y(tethered)	N	+++	+++	Small molecule/ion interactions	Tethering
Holography [41]	90 kDa	–	40 nM	80 nM	6.25 ms	N	Y	++	+++	Protein sizing	Below physiological concentration

(*Continued*)

Table 1. (*Continued*)

Technique	Detection limit: Achieved	Detection limit: Fundamental	Concentration: Low	Concentration: High	Temporal resolution: Minimal Interval	Temporal resolution: Long-term observation?	High-throughput?	Complexity: Resources	Complexity: Expertise	Applications	Limitation(s)
PNP[c]	43 kDa [42]		0.1 nM [43]	5 μM[44]	200 μs[44]	Y (3 mins) [45]	N	+	+++	Antibody detection [43,46] Conformational dynamics[45] SERS[47]	High salt concentration
FP–MC	1.2 kDa[48]		0.25 pM	15 pM	2 μs	N	Y	+	+++	Protein sizing Protein diffusion	Short observing duration Specialized expertise and resources

References: 1. (Yu *et al.*, 2016). 2. (Toropov *et al.*, 2023). 3. (Baaske *et al.*, 2014). 4. (Vincent *et al.*, 2020). 5. (Kim *et al.*, 2016). 6. (Yu et al. 2021). 7. (Babaei *et al.*, 2023). 8. (Wheaton and Gordon, 2015). 9. (Ying *et al.*, 2021). 10. (Hacohen *et al.*, 2018). 11. Yousefi *et al.*, 2023. 12. (Zehtabi-Oskuie *et al.*, 2013). 13. (Kotnala and Gordon, 2014a). 14. (Al Balushi and Gordon, 2014b). 15. (Al Balushi and Gordon, 2014a). 16. (Yousefi *et al.*, 2023). 17. (Pang and Gordon, 2012). 18. (Wheaton *et al.*, 2015). 19. (Dahmardeh *et al.*, 2023). 20. (Young *et al.*, 2018). 21. (Liebel *et al.*, 2017). 22. (Heermann *et al.*, 2021). 23. (Häußermann *et al.*, 2019. 24. (Taylor *et al.*, 2019). 25. (Fineberg *et al.*, 2020). 26. (Wu and Piszczek, 2020). 27. (Soltermann *et al.*, 2020). 28. (Sonn-Segev *et al.*, 2020). 29. (Foley *et al.*, 2021). 30. (Küppers *et al.*, 2023). 31. (Sun *et al.*, 2023). 32. (Zhang *et al.*, 2020). 33. (Wan *et al.*, 2022). 34. (Zhang *et al.*, 2022). 35. (Baaske *et al.*, 2022). 36. (Zhang *et al.*, 2021). 37. (Ma *et al.*, 2020). 38. (Špačková *et al.*, 2022). 39. (Peters *et al.*, 2023). 40. (Liang *et al.*, 2017). 41. (Thiele *et al.*, 2023). 42. (Alexandrakis *et al.*, 2020). 43. (Peri *et al.*, 2020). 44. (Verschueren *et al.*, 2019). 45. (Yang *et al.*, 2021). 46. (Peri *et al.*, 2020). 47. (Huang *et al.*, 2019). 48. (Needham *et al.*, 2024).

*iSCAT is the only technique commercialized. Data were taken from technical notes from Refeyn Ltd.

+In a physiological environment, proteins are typically present in the μM concentration range.

[a]Based on the authors' preliminary data.

[b]The duration is dependent on the channel length and the diffusion of protein.

[c]Plasmonic nanopores.

biotin binding (4 biotins per streptavidin), as well as modified biotin of different masses (Young *et al.*, 2018). The accuracy on these changes was at the kDa level and comparable to the change itself. Mass changes of lipid nanodisks and for proteins with glycosylation were also observed, as well as protein assembly by noting mass distributions with variations in protein concentration.

The scattered signal from single proteins in NOT experiments can be related to the size by the root mean squared deviation (RMSD) of the aperture transmission signal and the autocorrelation or power spectral density. The RMSD scales linearly with protein mass and gives the optical size similar to iScat (Wheaton and Gordon, 2015). The autocorrelation function measures the similarity between a signal and its time-delayed version, whereas the power spectral density function gives the distribution of average power in the frequency domain, and these are related through the Fourier transform. Equation 8 relates the corner frequency obtained from the power spectral density to the hydrodynamic radius to the power of −2/3 (Kotnala and Gordon, 2014b; Wheaton and Gordon, 2015; Babaei *et al.*, 2023). Interestingly, this expression contains both the optical size and the hydrodynamic size, r_h through the Stokes drag.

$$f_c = \frac{\kappa}{\gamma} \propto \frac{\alpha}{6\pi\eta r_h} \tag{8}$$

Sizing of single proteins with PSM revealed two size regimes: one for large nanoparticles that follows a $d^{5.6}$ size dependence and for smaller nanoparticles that follows d^3 size dependence. That method showed sizing down to single BSA proteins (66 kDa) (Ma *et al.*, 2020; Zhang *et al.*, 2020; Wan *et al.*, 2022; Zhang *et al.*, 2022). The molecular weight determination of single proteins using NSM was achieved through the integrated optical contrast being linearly dependent on the polarizability of the biomolecule, which is linearly dependent on the molecular weight. Similar to PSM, they detected a protein of 66 kDa while also being able to measure DNA and vesicles (Špačková *et al.*, 2022). The size sensitivity demonstrated for various techniques is shown in Figure 2.

Oligomers and assembly

iScat was used to measure oligomer species formation of the MinDE system by using a supported lipid bilayer (Heermann *et al.*, 2021). In the presence of ATP, MinD monomers were found to be the most prominent species in solution; however, on the lipid bilayer, MinD dimers were dominant. Although it should be noted that their imaging conditions do not allow for an accurate quantification of MinD monomers (33 kDa) on the lipid bilayer using iScat. At higher particle densities, they observed that MinD forms higher order-complexes on a crowded bilayer. Another study showed that the FWHM resolution of 20 kDa of iScat was able to resolve the oligomeric states of BSA, revealing the rare state of tetramers (0.25% abundance) (Hundt, 2021). Mass photometry has also been used to study the oligomeric equilibria of 2-cysteine peroxiredoxins in both humans and plants. Their results showed conserved features among both as well as species-specific features (Liebthal *et al.*, 2021). This technique has also been used to characterize immunoglobulin heavychain binding protein self-oligomerization and its dependence on temperature, showing the monomeric form is stabilized at higher temperature as well as ATP-induced monomer stabilization at low temperature (Rivera *et al.*, 2023).

https://doi.org/10.1017/S0033583524000088 Published online by Cambridge University Press

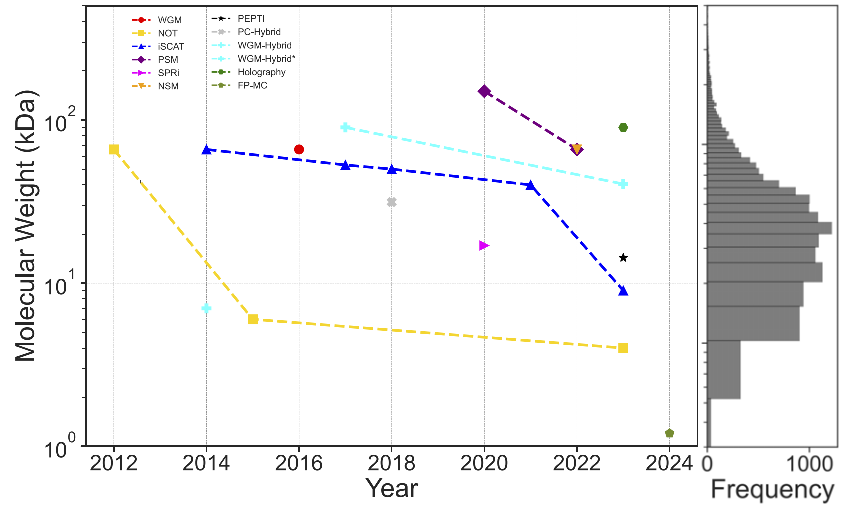

Figure 2. Molecular weight sensitivity of label-free single biomolecule technique advancements over time. Whispering gallery mode (WGM) (Yu *et al.*, 2016), nanoaperture optical tweezer (NOT) (Pang and Gordon, 2012; Wheaton and Gordon, 2015; Babaei *et al.*, 2023), interferometric scattering (iScat) (Piliarik and Sandoghdar, 2014; Liebel *et al.*, 2017; Young *et al.*, 2018; Hajdusits *et al.*, 2021; Dahmardeh *et al.*, 2023), plasmonic scattering microscopy (PSM) (Zhang *et al.*, 2020; Wan *et al.*, 2022), surface plasmon resonance imaging (SPRi) (Ma *et al.*, 2020), nanofluidic scattering microscopy (NSM) (Špačková *et al.*, 2022), plasmon enhanced protein tracking through interference (PEPTI) (Peters *et al.*, 2023), photonic-plasmonic hybrid (PC-Hybrid) (Liang *et al.*, 2017), plasmonic-WGM hybrid (WGM-Hybrid) (Kim *et al.*, 2017; Toropov *et al.*, 2023), WGM-Hybrid* measured nucleic acids (Baaske *et al.*, 2014), holography (Thiele *et al.*, 2023). Corresponding histogram of human proteome size/frequency is shown to the right (Consortium, 2019), FP-MC (Needham *et al.*, 2024).

NOTs have been used to probe the disassembly of single ferritin proteins under different pHs (Yousefi *et al.*, 2023). At pH 2, ferritin underwent a stepwise fragmentation with critical fragments occurring at dimer, tetramer, 12-mer, and 22-mer subunits.

Interactions

DNA-protein

Unzipping of 10 base pair DNA-hairpins was seen with tumor suppressor p53 protein-DNA complex, showing a longer DNA unzipping time than freely trapped DNA hairpins. A mutant p53-DNA complex was also trapped, showing that a single point mutation of Cys135Ser causes p53 to lose the ability to suppress DNA unzipping (Kotnala and Gordon, 2014a). Characterization of DNA binding with forkhead box protein P2 was performed using mass photometry and was compared with fluorescence proximity sensing, showing agreement with free energy measurements (Häußermann *et al.*, 2019).

Protein–protein

Quantification of affinities of tubulin monomers and heterodimers in the < µM range was shown using iScat (Fineberg *et al.*, 2020). That showed an αβ-tubulin dissociation constant of 8.48 ± 1.22 nM and, in the presence of GTP, a value of 3.69 ± 0.65 nM. The same group also showed that mass photometry was able to accurately count and distinguish proteins by molecular weight, revealing heterogeneity and abundances at the single molecule level (Soltermann *et al.*, 2020; Sonn-Segev *et al.*, 2020). Small molecules and Ions Single molecule dynamics of protein-small molecule interactions have been studied using NOTs (Al Balushi *et al.*, 2013; Al Balushi and Gordon, 2014a, 2014b; Yousefi *et al.*, 2023). Biotin-streptavidin, biotin-monovalent streptavidin, and acetylsalicylic acid-cyclooxygenase 2 were used to show that it is possible to distinguish between the bound and unbound state of the protein from the optical scattering (Al Balushi *et al.*, 2013; Al Balushi and Gordon, 2014b). Tolbutamide-human serum albumin and phenytoin-human serum albumin showed agreement in the dissociation constant reported in the literature by observing residence times represented by different amounts of transmission through the aperture (scattering) (Al Balushi and Gordon, 2014a). In a work looking at ferritin, real-time dynamics of iron loading and biomineralization within a single unlabelled protein complex were shown (Yousefi *et al.*, 2023). Differences in structural rigidity of the apo- and holo-ferritin were shown. In-situ iron loading was observed and attributed to the folding of 8 gated pores, causing dynamic instability while iron was loaded into the core of the protein. SPRi was used to study Ca^{2+} ions binding to calmodulin, showing that calcium binding altered the conformation of calmodulin, increasing the hydrodynamic radius by 13% (Ma *et al.*, 2020).

Antibody detection

Using a commercial mass photometry system (Refyn), the detection of CD16 and IgG binding was shown for one-site binding and human α-thrombin (HT) and monoclonal anti-HT for two-site binding. Association constants were calculated and showed good agreement with existing methods (Wu and Piszczek, 2020). Antibodies secreted from cells were monitored using iScat (McDonald *et al.*, 2018), finding the rate of secretion and the size range of secreted proteins and particles.

BSA and anti-BSA interactions were shown in a co-trapping experiment using NOTs (Zehtabi-Oskuie *et al.*, 2013). A variation of the NOT was used to discriminate the specific binding of anti-RAH to RAH antigen compared to non-specific binding of an anti-WNV antibody. That work integrated a nanopore with the double nanohole but showed that electrical measurements alone were not enough to discriminate between specific and non-specific binding, whereas it was possible with optical measurements. They were also able to quantify the dissociation constant to be 58 ± 17 nM (Peri *et al.*, 2019).

Conformational changes

The NOT trapping of BSA showed repeated steps that were attributed to conformational changes, as verified by reducing the pH and

https://doi.org/10.1017/S0033583524000088 Published online by Cambridge University Press

forcing the protein into the open state, where only a single step was seen at the higher transmission intensity (Pang and Gordon2012). Conformational changes were observed as steps in the transmitted intensity due to interactions for four different protein systems: haemoglobin interacting with single oxygen molecules, calmodulin under heating with increasing laser power (stabilized with calcium ions), adenylate kinase, and citrate synthase interacting with their substrates (Ying *et al.*, 2021). Variations in the extension of PR65 with various point mutations were measured with NOT and compared with theoretical predictions (Bahar *et al.*, 2023).

Diffusion and transport

The motion of myosin on actin filaments was tracked with iScat (Ortega Arroyo *et al.*, 2014). NSM and PEPTI tracked single, unlabelled protein diffusion. In NSM, the diffusivity was measured by the statistical analysis of the movement using a particle tracking algorithm. By approximating the protein as a hard neutral sphere, the hydrodynamic radius could also be inferred; however, the movement was inherently restricted by the nanochannel dimensions (Špačková *et al.*, 2022). Similarly, PEPTI measured the diffusion of proteins using a particle tracking algorithm, but likely due to the restriction of the protein being near a surface and strong optical and thermal forces, the measured diffusivity was smaller than expected from unconstrained 3D diffusion (Peters *et al.*, 2023).

Vibrational modes

Probing the acoustic vibrational modes in the range of 0.7–10 cm^{-1} for single proteins was achieved using NOTs in a technique named Extraordinary Acoustic Raman Spectroscopy (Wheaton *et al.*, 2015). Two identical lasers were used to trap the protein; one of the lasers was then thermally tuned to induce a small change in laser wavelength, creating a beat frequency between the two lasers. When the beat frequency was resonant with the proteins acoustic resonance, the protein was excited to oscillate resonantly, which increased scattered light intensity fluctuations. This technique was applied to conalbumin (76 kDa), cyclooxygenase (69 kDa), streptavidin (60 kDa), carbonic anhydrase (29 kDa), and trypsin inhibitor (21.5 kDa), with the measured acoustic modes matching well with theory (DeWolf and Gordon, 2016). This approach was also used to measure the vibrational modes of single-strand DNA of different lengths and bases, showing good agreement of the observed resonances with a simple 1D finite chain model (Kotnala *et al.*, 2015).

Conclusions and outlook

We have reviewed single-molecule techniques based on optical scattering, focusing on their wide applications in studying unmodified biomolecules. These techniques together can cover the size range of human proteins, with a detection limit down to 4 kDa (Babaei *et al.*, 2023). Currently, there are only a few approaches that can characterize individual, unmodified biomolecules in solution. Optical scattering is one primary approach. Other label-free techniques are mostly based on electrical measurements, including nanopores (Y.-L. Ying *et al.*, 2022; Wang *et al.*, 2021) , nanochannels (Choi *et al.*, 2021; Wang *et al.*, 2022), and nanowire field effect transistors (FETs) (Sorgenfrei *et al.*, 2011; He *et al.*, 2016; Liu *et al.*, 2023). While nanowire FETs typically require the analyte to be attached to the probe, they can detect single DNA signals without tethering when combined with nanopores (Xie *et al.*, 2012). Compared to light scattering approaches, nanopore sensing has been used in detecting a wider range of analytes, from subnanometers (metal ions (Roozbahani *et al.*, 2020) to hundreds of nanometers (virons (Taniguchi *et al.*, 2021). Nanopore's applications include DNA/RNA sequencing (Derrington *et al.*, 2010; Deamer *et al.*, 2016), protein fingerprinting (Yusko *et al.*, 2017; Houghtaling *et al.*, 2019) and protein sequencing (Hu *et al.*, 2021). Based on these applications, many companies have emerged, including Oxford Nanopore Technologies (Eisenstein, 2012), NabSys, and Figura Analytics and so forth. One challenge in nanopore sensing is that most proteins or DNA bases transit through the nanopore within several microseconds, too fast to be detected by the typical recording bandwidth (50 kHz (Houghtaling *et al.*, 2019), let alone to gather detailed information about the biomolecules. Recent efforts in electroosmotic trapping to slow down protein translocation have made it possible for nanopores to interrogate conformational changes of single proteins for longer durations (Galenkamp *et al.*, 2020; Huang *et al.*, 2020; Schmid *et al.*, 2021). Despite significant advancements, nanopore sensing can only operate at high salt concentrations (typically 1 M) due to its resistance pulse sensing nature.

Unlike nanopore sensing, only one optical scattering-based method has been commercialized - iScat, which was commercialized as Mass Photometry by Refeyn Ltd in 2018. With a brief period of time, Mass Photometry has led to over 300 research publications involving protein sizing, protein–protein interaction, and more. While each technique has distinct advantages and limitations, due to the nature of the scattering signal, most of them overlap in limitations such as low temporal resolution, low throughput, and restricted operating concentration ranges below the physiological environment. Moreover, the specialized expertise and resources required for most techniques can slow down their widespread adoption in biological laboratories.

Recent advances in machine-learning based data analysis keep pushing the detection limit of the single protein scattering signal (Dahmardeh *et al.*, 2023). Machine learning also offers potential to streamline data analysis (Thomsen *et al.*, 2020), which can facilitate the commercialization of the techniques by making them more user-friendly. High-speed cameras will promote optical scattering techniques in studying single proteins. On one hand, they improve the time resolution of the techniques that offer high-throughput, like iScat, SM, SPRi, PEPTi, and holography, allowing them to capture the fast interactions between different proteins or conformational changes within a single protein. On the other hand, replacing high-bandwidth photodetectors with high-speed cameras in the single-channel techniques, such as NOT, Opto-PSM, and PNP, may greatly improve the throughput of those techniques.

Integrating different optical scattering-based techniques has the potential to address some limitations. For example, NOTs collect a scattering signal only through an nanoaperture and at the same time reduce the sensing volume by plasmonic resonance, making it possible to operate at a concentration comparable to a physiological condition (e.g. micromolar (Wheaton and Gordon, 2015). However, NOTs suffer from the low throughput. PEPTi (Peters *et al.*, 2023), an approach combined NOT with iScat, shows promise in operating in high concentration while ensuring the throughput. Moreover, electrical signal-based approaches, such as the well-established nanopore technique, can offer complementary information to light scattering methods. Combining nanopores with NOTs has demonstrated potential for antibody detection (Peri *et al.*, 2019, 2020, DNA sequencing (Belkin *et al.*, 2015), single-molecule SERS (Huang *et al.*, 2019, and improving the capture rate of NOTs (Verschueren *et al.*, 2019. The integration of iScat with

https://doi.org/10.1017/S0033583524000088 Published online by Cambridge University Press

nanochannels, forming NSM, shows promise in analysing complex biofluid samples (Špačková *et al.*, 2022).

In the past decades, FRET (Schuler, 2013; Lerner *et al.*, 2018) and single-molecule force spectroscopy (Schönfelder *et al.*, 2016; Li, 2023) have revolutionized the field of protein study and revealed features that are hidden in ensemble-level measurements (Michalet *et al.*, 2006; Ziemba *et al.*, 2014; Willkomm *et al.*, 2022). Label-free methods, particularly techniques based on optical scattering reviewed here, provide additional information beyond the labelled techniques. Given the groundbreaking research in complex protein samples (Heermann *et al.*, 2021), long-term observation of some molecules by NOTs (Pang and Gordon, 2012; Yousefi *et al.*, 2023, plasmonic nanopores (Peri *et al.*, 2020), and imaging macromolecules in live cells (Zhang *et al.*, 2021; Ma *et al.*, 2022; Küppers *et al.*, 2023), we believe that light-scattering based techniques will provide game-changing advances to life sciences.

Competing interest. The authors declare none.

References

Al Balushi AA and Gordon R (2014a) A label-free untethered approach to single-molecule protein binding kinetics. *Nano Letters* **14**(10), 5787–5791.

Al Balushi AA and Gordon R (2014b) Label-free free-solution single-molecule protein–small molecule interaction observed by double nanohole plasmonic trapping. *ACS Photonics* **1**(5), 389–393.

Al Balushi AA, Zehtabi-Oskuie A and Gordon R (2013) Observing single protein binding by optical transmission through a double nanohole aperture in a metal film. *Biomedical Optics Express* **4**(9), 1504–1511.

Alexandrakis G, Sasank Peri SS, Subnani MK, Raza UM, Ghaffari S, Lee JS, Kim MJ, and Weidanz J (2020) Quantification of low-affinity kinetics between cancer immunity relevant ligands and natural killer cell receptors with a self-induced back-action actuated nanopore electrophoresis (sane) sensor. In *Optical Trapping and Optical Micromanipulation* **xvii**, 11463, 1146306.

Armani AM, Kulkarni RP, Fraser SE, Flagan RC and Vahala KJ (2007) Label-free, single-molecule detection with optical microcavities. *Science* **317**(5839), 783–787.

Arnold S, Khoshsima M, Iwao Teraoka SH and Vollmer F (2003) Shift of whispering-gallery modes in microspheres by protein adsorption. *Optics Letters* **28**(4), 272–274.

Arviv O and Levy Y (2012) Folding of multidomain proteins: Biophysical consequences of tethering even in apparently independent folding. *Proteins: Structure, Function, and Bioinformatics* **80**(12), 2780–2798.

Baaske M, Asgari N, Punj D, and Orrit M (2022) Nanosecond time scale transient optoplasmonic detection of single proteins. *Science Advances* **8**(2), eabl5576.

Baaske MD, Foreman MR and Vollmer F (2014) Single-molecule nucleic acid interactions monitored on a label-free microcavity biosensor platform. *Nature Nanotechnology* **9**(11), 933–939.

Babaei E, Wright D and Gordon R (2023) Fringe dielectrophoresis nanoaperture optical trapping with order of magnitude speed-up for unmodified proteins. *Nano Letters* **23**(7), 2877–2882.

Bahar I, Banerjee A, Mathew S, Naqvi M, Yilmaz S, Zachoropoulou M, Doruker P, Kumita J, Yang S-H, Gur M, Itzhaki L and Gordon R (2023) Influence of point mutations on PR65 conformational adaptability: Insights from nanoaperture optical tweezer experiments and molecular simulations. *Science Advances* **10**, eadn2208.

Becker J, Peters JS, Crooks I, Helmi S, Synakewicz M, Schuler B and Kukura P (2023) A quantitative description for optical mass measurement of single biomolecules. *ACS Photonics* **10**(8), 2699–2710.

Belkin M, Chao S-H, Jonsson MP, Dekker C and Aksimentiev A (2015) Plasmonic nanopores for trapping, controlling displacement, and sequencing of DNA. *ACS Nano* **9**(11), 10598–10611.

Bobbert PA and Vlieger J (1987) The polarizability of a spheroidal particle on a substrate. *Physica A: Statistical Mechanics and its Applications* **147**(1–2), 115–141.

Busto MD (1998) An experiment illustrating the effect of immobilisation on enzyme properties. *Biochemical Education* **26**(4), 304–308.

Carmichael SP and Shell MS (2015) Entropic (de) stabilization of surface-bound peptides conjugated with polymers. *The Journal of Chemical Physics* **143**(24).

Choi J, Jia Z, Riahipour R, McKinney CJ, Amarasekara CA, Weerakoon-Ratnayake KM, Soper SA and Park S (2021) Label-free identification of single mononucleotides by nanoscale electrophoresis. *Small* **17**(42), 2102567.

Chung HS, McHale K, Louis JM and Eaton WA (2012) Single-molecule fluorescence experiments determine protein folding transition path times. *Science* **335**(6071), 981–984.

Dahmardeh M, Dastjerdi HM, Mazal H, Köstler H and Sandoghdar V (2023) Self-supervised machine learning pushes the sensitivity limit in label-free detection of single proteins below 10 kda. *Nature Methods* **20**(3), 442–447.

Dantham VR, Holler S, Barbre C, Keng D, Kolchenko V and Arnold S (2013) Label-free detection of single protein using a nanoplasmonic-photonic hybrid microcavity. *Nano Letters* **13**(7), 3347–3351.

Dastjerdi HM, Dahmardeh M, Gemeinhardt A, Mahmoodabadi RG, Köstler H and Sandoghdar V (2021) Optimized analysis for sensitive detection and analysis of single proteins via interferometric scattering microscopy. *Journal of Physics D: Applied Physics* **55**(5), 054002.

Deamer D, Akeson M and Branton D (2016) Three decades of nanopore sequencing. *Nature Biotechnology* **34**(5), 518–524.

Derrington IM, Butler TZ, Collins MD, Manrao E, Pavlenok M, Niederweis M and Gundlach JH (2010) Nanopore DNA sequencing with MspA. *Proceedings of the National Academy of Sciences* **107**(37), 16060–16065.

DeWolf T and Gordon R (2016) Theory of acoustic Raman modes in proteins. *Physical Review Letters* **117**(13), 138101.

Dietz MS, Wehrheim SS, Harwardt M-LIE, Niemann HH and Heilemann M (2019) Competitive binding study revealing the influence of fluorophore labels on biomolecular interactions. *Nano Letters* **19**(11), 8245–8249.

Diezmann Lv, Shechtman Y and Moerner WE (2017) Three-dimensional localization of single molecules for super-resolution imaging and single-particle tracking. *Chemical Reviews* **117**(11), 7244–7275.

Eisenstein M (2012) Oxford nanopore announcement sets sequencing sector abuzz. *Nature Biotechnology* **30**(4), 295–296.

Filipe V, Hawe A and Jiskoot W (2010) Critical evaluation of nanoparticle tracking analysis (NTA) by nanosight for the measurement of nanoparticles and protein aggregates. *Pharmaceutical Research* **27**, 796–810.

Fineberg A, Surrey T and Kukura P (2020) Quantifying the monomer–dimer equilibrium of tubulin with mass photometry. *Journal of Molecular Biology* **432**(23), 6168–6172.

Foley EDB, Kushwah MS, Young G, and Kukura P (2021) Mass photometry enables label-free tracking and mass measurement of single proteins on lipid bilayers. *Nature Methods* **18**(10), 1247–1252.

Foley KJ, Shan X and Tao NJ (2008) Surface impedance imaging technique. *Analytical Chemistry* **80**(13), 5146–5151.

Franke S, Ren J and Hughes S (2023) Impact of mode regularization for quasinormalmode perturbation theories. *Physical Review A* **108**(4), 043502.

Galenkamp NS, Biesemans A and Maglia G (2020) Directional conformer exchange in dihydrofolate reductase revealed by single-molecule nanopore recordings. *Nature Chemistry* **12**(5), 481–488.

Grawe RW and Knotts TA (2017) The effects of tether placement on antibody stability on surfaces. *The Journal of Chemical Physics* **146**(21), 215102.

Ha T (2014) Single-molecule methods leap ahead. *Nature Methods* **11**(10), 1015–1018.

Hacohen N, Ip CJX, and Gordon R (2018) Analysis of egg white protein composition with double nanohole optical tweezers. *ACS Omega* **3**(5), 5266–5272.

Hajdusits B, Suskiewicz MJ, Hundt N, Meinhart A, Kurzbauer R, Leodolter J, Kukura P and Clausen T (2021) McsB forms a gated kinase chamber to mark aberrant bacterial proteins for degradation. *eLife* **10**, e63505.

Hanefeld U, Cao L and Magner E (2013) Enzyme immobilisation: Fundamentals and application. *Chemical Society Reviews* **42**(15), 6211–6212.

Hanson JA, Duderstadt K, PWatkins L, Bhattacharyya S, Brokaw J, Chu J-W and Yang H (2007) Illuminating the mechanistic roles of enzyme conformational dynamics. *Proceedings of the National Academy of Sciences* **104**(46), 18055–18060.

Häußermann K, Young G, Kukura P and Dietz H (2019) Dissecting FOXP2 oligomerization and dna binding. *Angewandte Chemie* **131**(23), 7744–7749.

He G, Li J, Ci H, Qi C and Guo X (2016) Direct measurement of single-molecule DNA hybridization dynamics with single-base resolution. *Angewandte Chemie* **128**(31), 9182–9186.

Heermann T, Steiert F, Ramm B, Hundt N and Schwille P (2021) Mass-sensitive particle tracking to elucidate the membrane-associated minde reaction cycle. *Nature Methods* **18**(10), 1239–1246.

Henzler-Wildman KA, Thai V, Lei M, Ott M, MagnusWolf-Watz TF, Pozharski E, Wilson MA, Petsko GA, Karplus M, Hübner CG and Kern D (2007) Intrinsic motions along an enzymatic reaction trajectory. *Nature* **450** (7171), 838–844.

Houghtaling J, Ying C, Eggenberger OM, Fennouri A, Nandivada S, Acharjee M, Li J, Hall AR and Mayer M (2019) Estimation of shape, volume, and dipole moment of individual proteins freely transiting a synthetic nanopore. *ACS Nano* **13**(5), 5231–5242.

Hu Z-L, Huo M-Z, Ying Y-L and Long Y-T (2021) Biological nanopore approach for single-molecule protein sequencing. *Angewandte Chemie* **133** (27), 14862–14873.

Huang J-A, Mousavi MZ, Zhao Y, Hubarevich A, Omeis F, Giovannini G, Schütte M, Garoli D and Angelis FD (2019) Sers discrimination of single dna bases in single oligonucleotides by electro-plasmonic trapping. *Nature Communications* **10**(1), 5321.

Huang G, Willems K, Bartelds M, Van Dorpe P, Soskine M and Maglia G (2020) Electro-osmotic vortices promote the capture of folded proteins by PlyAB nanopores. *Nano Letters* **20**(5), 3819–3827.

Hughes LD, Rawle RJ and Boxer SG (2014) Choose your label wisely: Water-soluble fluorophores often interact with lipid bilayers. *PLoS One* **9**(2), e87649.

Hundt N (2021) Label-free, mass-sensitive single-molecule imaging using interferometric scattering microscopy. *Essays in Biochemistry* **65**(1), 81–91.

Ilari A and Savino C (2008) Protein structure determination by x-ray crystallography. *Bioinformatics: Data, Sequence Analysis and Evolution* **452**, 63–87.

Jiang Q, Rogez B, Claude J-B, Moreau A, Lumeau J, Baffou G and Wenger J (2020) Adhesion layer influence on controlling the local temperature in plasmonic gold nanoholes. *Nanoscale* **12**(4), 2524–2531.

Kay LE (2011) NMR studies of protein structure and dynamics. *Journal of Magnetic Resonance* **213**(2), 477–491.

Kim E, Baaske MD, Schuldes I, Wilsch PS and Vollmer F (2017) Label-free optical detection of single enzyme-reactant reactions and associated conformational changes. *Science Advances* **3**(3), e1603044.

Kim E, Baaske MD, and Vollmer F (2016) In situ observation of single-molecule surface reactions from low to high affinities. *Advanced Materials* **28**, 9941–9948.

Kotnala A and Gordon R (2014a) Double nanohole optical tweezers visualize protein p53 suppressing unzipping of single DNA-hairpins. *Biomedical Optics Express* **5**(6), 1886–1894.

Kotnala A and Gordon R (2014b) Quantification of high-efficiency trapping of nanoparticles in a double nanohole optical tweezer. *Nano Letters* **14**(2), 853–856.

Kotnala A, Wheaton S and Gordon R (2015) Playing the notes of dna with light: Extremely high frequency nanomechanical oscillations. *Nanoscale* **7**(6), 2295–2300.

Kristensen PT and Hughes S (2014) Modes and mode volumes of leaky optical cavities and plasmonic nanoresonators. *ACS Photonics* **1**(1), 2–10.

Küppers M, Albrecht D, Kashkanova AD, Lühr J and Sandoghdar V (2023) Confocal interferometric scattering microscopy reveals 3D nanoscopic structure and dynamics in live cells. *Nature Communications* **14**(1), 1962.

Lerner E, Cordes T, Ingargiola A, Alhadid Y, Chung SY, Michalet X and Weiss S (2018) Toward dynamic structural biology: Two decades of single-molecule förster resonance energy transfer. *Science* **359**(6373), eaan1133.

Levy Y (2017) Protein assembly and building blocks: Beyond the limits of the LEGO brick metaphor. *Biochemistry* **56**(38), 5040–5048.

Li H (2023) Single molecule force spectroscopy studies on metalloproteins: Opportunities and challenges. *Langmuir* **39**(4), 1345–1353.

Li D, Liu MS and Ji B (2015) Mapping the dynamics landscape of conformational transitions in enzyme: The adenylate kinase case. *Biophysical Journal* **109**(3), 647–660.

Li Y, Struwe WB and Kukura P (2020) Single molecule mass photometry of nucleic acids. *Nucleic Acids Research* **48**(17), e97–e97.

Liang F, Guo Y, Hou S and Quan Q (2017) Photonic-plasmonic hybrid single molecule nanosensor measures the effect of fluorescent labels on DNA-protein dynamics. *Science Advances* **3**(5), e1602991.

Liebel M, Hugall JT and Van Hulst NF (2017) Ultrasensitive label-free nanosensing and high-speed tracking of single proteins. *Nano Letters* **17**(2), 1277–1281.

Liebthal M, Kushwah MS, Kukura P and Dietz K-J (2021) Single molecule mass photometry reveals the dynamic oligomerization of human and plant peroxiredoxins. *IScience* **24**(11), 103258.

Liu W, Chen L, Yin D, Yang Z, Feng J, Sun Q, Lai L and Guo X (2023) Visualizing single-molecule conformational transition and binding dynamics of intrinsically disordered proteins. *Nature Communications* **14**(1), 5203.

Liu X-W, Yang Y, Wang W, Wang S, Gao M, Wu J and Tao N (2017) Plasmonic-based electrochemical impedance imaging of electrical activities in single cells. *Angewandte Chemie International Edition* **56**(30), 8855–8859.

Lu T, Lee H, Chen T, Herchak S, Kim J-H, Fraser SE, Flagan RC and Vahala K (2011) High sensitivity nanoparticle detection using optical microcavities. *Proceedings of the National Academy of Sciences* **108**(15), 5976–5979.

Luo W, Dai Y, Chen Z, Yue X, Andrade-Powell KC and Chang J (2020) Spatial and temporal tracking of cardiac exosomes in mouse using a nano-luciferase-CD63 fusion protein. *Communications Biology* **3**(1), 114.

Ma G, Zhang P, Zhou X, Wan Z and Wang S (2022) Label-free single molecule pulldown for the detection of released cellular protein complexes. *ACS Central Science* **8**(9), 1272–1281.

Ma G, ZijianWan YY, Zhang P, Wang S and Tao N (2020) Optical imaging of single-protein size, charge, mobility, and binding. *Nature Communications* **11**(1), 4768.

Martin-Baniandres P, Lan WH, Board S, Romero-Ruiz M, Garcia-Manyes S, Qing Y and Bayley H (2023) Enzyme-less nanopore detection of post translational modifications within long polypeptides. *Nature Nanotechnology* **18**, 1335–1340.

McDonald MP, Gemeinhardt A, König K, Piliarik M, Schaffer S, Völkl S, Aigner M, Mackensen A and Sandoghdar V (2018) Visualizing single-cell secretion dynamics with single-protein sensitivity. *Nano Letters* **18**(1), 513–519.

Michalet X, Weiss S and Jäger M (2006) Single-molecule fluorescence studies of protein folding and conformational dynamics. *Chemical Reviews* **106**(5), 1785–1813.

Miller H, Zhou Z, Shepherd J, JMWollman A and Leake MC (2017) Single-molecule techniques in biophysics: A review of the progress in methods and applications. *Reports on Progress in Physics* **81**(2), 024601.

Moerner WE (2002) A dozen years of single-molecule spectroscopy in physics, chemistry, and biophysics. *The Journal of Physical Chemistry B* **106**, 910–927.

Needham LM, Saavedra C, Rasch JK, Barber D, Schweitzer B, Fairhall A, Vollbrecht C, Wan S, Podorova Y, Bergsten A, Mehlenbacher B, Zhang Z, Tenbrake L, Saimi J, Kneely L, Kirkwood J, Pfeifer H, Chapman E and Goldsmith R (2024) Label-free detection and profiling of individual solution-phase molecules. *Nature* **629**, 1062–1068.

Ortega Arroyo J, Andrecka J, Spillane KM, Billington N, Takagi Y, Sellers JR and Kukura P (2014) Label-free, all-optical detection, imaging, and tracking of a single protein. *Nano Letters* **14**(4), 2065–2070.

Ortiz-Orruño U, Quidant R, van Hulst NF, Liebel M and Arroyo JO (2022) Simultaneous sizing and refractive index analysis of heterogeneous nanoparticle suspensions. *ACS Nano* **17**(1), 221–229.

Pang Y and Gordon R (2012) Optical trapping of a single protein. *Nano Letters* **12**(1), 402–406.

Peri SSS, Sabnani MK, Raza MU, Ghaffari S, Gimlin S, Wawro DD, Lee JS, Kim MJ, Weidanz J and Alexandrakis G (2019) Detection of specific antibody-ligand interactions with a self-induced back-action actuated nanopore electrophoresis sensor. *Nanotechnology* **31**(8), 085502.

Peri SSS, Sabnani MK, Raza MU, Urquhart EL, Ghaffari S, Lee JS, Kim MJ, Weidanz J and Alexandrakis G (2020) Quantification of low affinity binding interactions between natural killer cell inhibitory receptors and targeting ligands with a self-induced back-action actuated nanopore electrophoresis (SANE) sensor. *Nanotechnology* **32**(4), 045501.

Peters M, McIntosh D, Albu AB, Ying C and Gordon R (2023) Label-free tracking of proteins through plasmon enhanced interference. *ACS Nanoscience Au* **4**(1), 69–75.

Piliarik M and Sandoghdar V (2014) Direct optical sensing of single unlabelled proteins and super resolution imaging of their binding sites. *Nature Communications* **5**(1), 4495.

Reja SI, Minoshima M, Hori Y and Kikuchi K (2021) Near-infrared fluorescent probes: A next-generation tool for protein-labeling applications. *Chemical Science* **12**(10), 3437–3447.

Riback JA, Bowman MA, Zmyslowski AM, KevinWPlaxco PLC and Sosnick TR (2019) Commonly used FRET fluorophores promote collapse of an otherwise disordered protein. *Proceedings of the National Academy of Sciences* **116**(18), 8889–8894.

Ringe D and Petsko GA (1985) Mapping protein dynamics by X-ray diffraction. *Progress in Biophysics and Molecular Biology* **45**(3), 197–235.

Rivera M, Burgos-Bravo F, Engelberger F, Asor R, Lagos-Espinoza MIA, Figueroa M, Kukura P, Ramírez-Sarmiento CA, Baez M, Smith SB and Wilson CAM (2023) Effect of temperature and nucleotide on the binding of Bip chaperone to a protein substrate. *Protein Science* **32**(7), e4706.

Rodrigues RC, Ortiz C, Berenguer-Murcia Á, Torres R and Fernández-Lafuente R (2013) Modifying enzyme activity and selectivity by immobilization. *Chemical Society Reviews* **42**(15), 6290–6307.

Roozbahani GM, Chen X, Zhang Y, Wang L and Guan X (2020) Nanopore detection of metal ions: Current status and future directions. *Small Methods* **4** (10), 2000266.

Schmid S and Dekker C (2021) The neotrap–en route with a new single-molecule technique. *IScience* **24**(10), 1003007.

Schmid S, Stömmer P, Dietz H and Dekker C (2021) Nanopore electro-osmotic trap for the label-free study of single proteins and their conformations. *Nature Nanotechnology* **16**(11), 1244–1250.

Schönfelder J, Sancho DD and Perez-Jimenez R (2016) The power of force: Insights into the protein folding process using single-molecule force spectroscopy. *Journal of Molecular Biology* **428**(21), 4245–4257.

Schuler B (2013) Single-molecule fret of protein structure and dynamics-a primer. *Journal of Nanobiotechnology* **11**(1), 1–17.

Shan X, Patel U, Wang S, Iglesias R and Tao N (2010) Imaging local electrochemical current via surface plasmon resonance. *Science* **327**(5971), 1363–1366.

Shental-Bechor D and Levy Y (2008) Effect of glycosylation on protein folding: A close look at thermodynamic stabilization. *Proceedings of the National Academy of Sciences* **105**(24), 8256–8261.

Soltermann F, Foley EDB, Pagnoni V, Galpin M, Benesch JLP, Kukura P and Struwe WB (2020) Quantifying protein protein interactions by molecular counting with mass photometry. *Angewandte Chemie International Edition* **59**(27), 10774–10779.

Sonn-Segev A, Belacic K, Bodrug T, Young G, VanderLinden RT, Schulman BA, Schimpf J, Friedrich T, Dip PV, Schwartz TU, Bauer B, Peters JM, Struwe WB, Benesch JLP, Brown NG, Haselbach D and Kukura P (2020) Quantifying the heterogeneity of macromolecular machines by mass photometry. *Nature Communications* **11**(1), 1772.

Sorgenfrei S, Chiu C-y, Ruben L, Yu Y-J, Kim P, Nuckolls C and Shepard KL (2011) Label-free single-molecule detection of dna-hybridization kinetics with a carbon nanotube field-effect transistor. *Nature Nanotechnology* **6**(2), 126–132.

Špačková B, Moberg HK, Fritzsche J, Tenghamn J, Sjösten G, Šıpová-Jungová H, Albinsson D, Lubart Q, van Leeuwen D, Westerlund F, Midtvedt D, Esbjörner EK, Käll M, Volpe G and Langhammer C (2022) Label-free nanofluidic scattering microscopy of size and mass of single diffusing molecules and nanoparticles. *Nature Methods* **19**(6), 751–758.

Su J, Goldberg AFG and Stoltz BM (2016) Label-free detection of single nanoparticles and biological molecules using microtoroid optical resonators. *Light: Science & Applications* **5**(1), e16001–e16001.

Sun YS, Landry JP, Fei YY, Zhu XD, Luo JT, Wang XB and Lam KS (2008) Effect of fluorescently labeling protein probes on kinetics of protein- ligand reactions. *Langmuir* **24**(23), 13399–13405.

Sun Y, Wang J, Zeng Q, Yang Y, Zhang C, Li J and Yu H (2023) Integral scattering microscopy of single molecules beyond quantum noise limit. chemrxiv.

Taniguchi M, Minami S, Ono C, Hamajima R, Morimura A, Hamaguchi S, Akeda Y, Kanai Y, Kobayashi T, Kamitani W, Terada Y, Suzuki K, Hatori N, Yamagishi Y, Washizu N, Takei H, Sakamoto O, Naono N, Tatematsu K, Washio T, Matsuura Y and Tomono K (2021) Combining machine learning and nanopore construction creates an artificial intelligence nanopore for coronavirus detection. *Nature Communications* **12**(1), 3726.

Taylor RW, Mahmoodabadi RG, Rauschenberger V, Giessl A, Schambony A, and Sandoghdar V (2019) Interferometric scattering microscopy reveals microsecond nanoscopic protein motion on a live cell membrane. *Nature Photonics* **13**(7), 480–487.

Thiele JC, Pfitzner E and Kukura P (2023) Single-protein optical holography. *Nature Photonincs* **18**, 388–395.

Thomsen J, Sletfjerding MB, Jensen SB, Stella S, Paul B, Malle MG, Montoya G, Petersen TC and Hatzakis NS (2020) Deepfret, a software for rapid and automated single-molecule fret data classification using deep learning. *eLife* **9**, e60404.

Toropov NA, Houghton MC, Yu D and Vollmer F (2023) Thermo-optoplasmonic single-molecule sensing on optical microcavities. *ACS Nano* **18**(27), 17534–17546.

Uniprot Consortium (2019) Uniprot: A worldwide hub of protein knowledge. *Nucleic Acids Research* **47**(D1), D506–D515.

Verschueren DV, Pud S, Shi X, Lorenzo De Angelis LK and Dekker C (2018) Label-free optical detection of DNA translocations through plasmonic nanopores. *ACS Nano* **13**(1), 61–70.

Verschueren D, Shi X and Dekker C (2019) Nano-optical tweezing of single proteins in plasmonic nanopores. *Small Methods* **3**(5), 1800465.

Vincent S, Subramanian S, and Vollmer F (2020) Optoplasmonic characterisation of reversible disulfide interactions at single thiol sites in the attomolar regime. *Nature Communications* **11**(1), 2043.

Wan Z, Ma G, Zhang P and Wang S (2022) Single-protein identification by simultaneous size and charge imaging using evanescent scattering microscopy. *ACS Sensors* **7**(9), 2625–2633.

Wang Y, ZequnWang LW, Tong T, Zhang X, Fang S, Xie W, Liang L, Yin B, Yuan J, Zhang J and Wang D (2022) Comparison study on single nucleotide transport phenomena in carbon nanotubes. *Nano Letters* **22**(5), 2147–2154.

Wang Y, Zhao Y, Bollas A, Wang Y and Au KF (2021) Nanopore sequencing technology, bioinformatics and applications. *Nature Biotechnology* **39**(11), 1348–1365.

Weisgerber AW and Knowles MK (2021) Membrane dynamics are slowed for Alexa594-labeled membrane proteins due to substrate interactions. *BBA Advances* **1**, 100026.

Wheaton S, Gelfand RM and Gordon R (2015) Probing the raman-active acoustic vibrations of nanoparticles with extraordinary spectral resolution. *Nature Photonics* **9**(1), 68–72.

Wheaton S and Gordon R (2015) Molecular weight characterization of single globular proteins using optical nanotweezers. *Analyst* **140**(14), 4799–4803.

Willkomm S, Jakob L, Kramm K, Graus V, Neumeier J, Meister G and Grohmann D (2022) Single-molecule fret uncovers hidden conformations and dynamics of human argonaute 2. *Nature Communications* **13**(1), 3825.

Wu T, Gurioli M and Lalanne P (2021) Nanoscale light confinement: The Q's and V's. *ACS Photonics* **8**(6), 1522–1538.

Wu D and Piszczek G (2020) Measuring the affinity of protein-protein interactions on a single-molecule level by mass photometry. *Analytical Biochemistry* **592**, 113575.

Xie P, Xiong Q, Fang Y, Qing Q and MLieber C (2012) Local electrical potential detection of DNA by nanowire–nanopore sensors. *Nature Nanotechnology* **7**(2), 119–125.

Xu Z, Song W and Crozier KB (2018) Direct particle tracking observation and Brownian dynamics simulations of a single nanoparticle optically trapped by a plasmonic nanoaperture. *ACS Photonics* **5**(7), 2850–2859.

Yang W, van Dijk M, Primavera C and Dekker C (2021) Fib-milled plasmonic nanoapertures allow for long trapping times of individual proteins. *iScience* **24**(11), 103237.

Yin L, Wang W, Wang S, Zhang F, Zhang S and Tao N (2015) How does fluorescent labeling affect the binding kinetics of proteins with intact cells? *Biosensors and Bioelectronics* **66**, 412–416.

Ying Y-L, Hu Z-L, Zhang S, YujiaQing AF, Maglia G, Meller A, Bayley H, Dekker C and Long Y-T (2022) Nanopore-based technologies beyond dna sequencing. *Nature Nanotechnology* **17**(11), 1136–1146.

Ying C, Karakaci E, Bermudez-Urena E, Ianiro A,Foster C, Awasthi S, Guha A, Bryan L, List J, Balog S, Acuna GP, Gordon R and Mayer M (2021) Watching single unmodified enzymes at work. arXiv: 2107.06407 [physics.bio-ph].

Yoo D, Gurunatha KL, Choi H-K, Mohr DA, Ertsgaard CT, Gordon R and Oh S-H (2018) Low-power optical trapping of nanoparticles and proteins with resonant coaxial nanoaperture using 10 nm gap. *Nano Letters* **18**(6), 3637–3642.

Young G, Hundt N, Cole D, Fineberg A, Andrecka J, Tyler A, Olerinyova A, Ansari A, Marklund E, Collier M, Chandler S, Tkachenko O, Allen J, Crispin M, Billington N, Takagi Y, Sellers J, Eichmann C, Selenko P, Frey L, Riek R, Galpin M, Struwe W, Benesch J and Kukura P (2018) Quantitative mass imaging of single biological macromolecules. *Science* **360**(6387), 423–427.

Yousefi A, Ying C, Parmenter CDJ, Assadipapari M, Sanderson G, Zheng Z, Xu L, Zargarbashi S, Hickman GJ, Cousins RB, Mellor CJ, Mayer M and Rahmani M (2023) Optical monitoring of in situ iron loading into single, native ferritin proteins. *Nano Letters* **23**(8), 3251–3258.

Yousefi A, Zheng Z, Zargarbashi S, Assadipapari M, Hickman GJ, Parmenter CDJ, Bueno-Alejo CJ, Sanderson G, Craske D, Xu L, Perry CC, Rahmani M and Ying C. (2023) Structural flexibility and disassembly kinetics of single ferritins using optical nanotweezers. bioRxiv, 2023–09.

Yu D, Humar M, Meserve K, Bailey RC, Chormaic SN, and Vollmer F (2021) Whispering-gallery-mode sensors for biological and physical sensing. *Nature Reviews Methods Primers* **1**(1), 83.

Yu W, Jiang WC, Lin Q and Lu T (2016) Cavity optomechanical spring sensing of single molecules. *Nature Communications* **7**(1), 12311.

Yusko EC, Bruhn BR, OliviaMEggenberger JH, Rollings RC, Walsh NC, Nandivada S, Pindrus M, Hall AR, Sept D, Li J, Kalonia DS and Mayer M (2017) Real-time shape approximation and fingerprinting of single proteins using a nanopore. *Nature Nanotechnology* **12**(4), 360–637.

Zanetti-Domingues LC, Tynan CJ, Rolfe DJ, Clarke DT and Martin-Fernandez M (2013) Hydrophobic fluorescent probes introduce artifacts into single molecule tracking experiments due to non-specific binding. *PLoS One* **8**(9), e74200.

Zehtabi-Oskuie A, Jiang H, Cyr BR, Rennehan DW, Al-Balushi AA and Gordon R (2013) Double nanohole optical trapping: Dynamics and protein-antibody co-trapping. *Lab on a Chip* **13**(13), 2563–2568.

Zhang P, Ma G, Dong W, Wan Z, Wang S and Tao N (2020) Plasmonic scattering imaging of single proteins and binding kinetics. *Nature Methods* **17** (10), 1010–1017.

Zhang P, Zhou X, Wang R, Jiang J, Wan Z and Wang S (2021) Label-free imaging of nanoscale displacements and free energy profiles of focal adhesions with plasmonic scattering microscopy. *ACS Sensors* **6**(11), 4244–4254.

Zhang P, Zhou L, Wang R, Zhou X, Jiang J, Wan Z and Wang S (2022) Evanescent scattering imaging of single protein binding kinetics and DNA conformation changes. *Nature Communications* **13**(1), 2298.

Ziemba BP, Li J, Landgraf KE, Knight JD, Voth GA and Falke JJ (2014) Single-molecule studies reveal a hidden key step in the activation mechanism of membrane-bound protein kinase c-α. *Biochemistry* **53**(10), 1697–1713.

Zijlstra P, Paulo PMR and Orrit M (2012) Optical detection of single non-absorbing molecules using the surface plasmon resonance of a gold nanorod. *Nature Nanotechnology* **7**(6), 379–382.

https://doi.org/10.1017/S0033583524000088 Published online by Cambridge University Press